A Current-Transient Methodology for Trap Analysis for GaN High Electron Mobility Transistors

Jungwoo Joh and Jesús A. del Alamo

***Abstract*—Trapping is one of the most deleterious effects that limit performance and reliability in GaN HEMTs. In this paper, we present a methodology to study trapping characteristics in GaN HEMTs that is based on current-transient measurements. Its uniqueness is that it is amenable to integration with electrical stress experiments in long-term reliability studies. We present the details of the measurement and analysis procedures. With this method, we have investigated the trapping and detrapping dynamics of GaN HEMTs. In particular, we examined layer location, energy level, and trapping/detrapping time constants of dominant traps. We have identified several traps inside the AlGaN barrier layer or at the surface close to the gate edge and in the GaN buffer.**

***Index Terms*—GaN, high-electron mobility transistors (HEMTs), measurement, transient, trapping.**

I. Introduction

GaN high-electron mobility transistors (HEMTs) have demonstrated outstanding performance in RF power and high-voltage switching applications [1], [2]. One of the most deleterious mechanisms that limit the performance and reliability in GaN HEMTs is the prominent trapping effect [3]. The so-called "current collapse"—a recoverable temporary reduction in drain current after the application of a high voltage—is perhaps the best known of these trapping phenomena.

In the ON-state, hot electrons from the channel can gain enough energy to overcome the energy barrier that exists in the extrinsic region of an AlGaN/GaN HEMT and get trapped at the surface or inside the AlGaN barrier itself [4], [5]. These trapped electrons change the electrostatics such that they deplete the channel carrier concentration in the extrinsic drain, resulting in a reduction of the drain current [6]. Although the trapping at the surface or inside the AlGaN barrier layer is believed to be important in current collapse, it has also been postulated that electron trapping in the GaN buffer can cause it [3]. This type of current collapse was not observed in devices built on a conducting buffer layer [3]. On the other hand, in the OFF-state under high V_{DG}, surface states between the gate and the drain can trap electrons that tunnel from the gate metal [6]–[8]. Consistent with this kind of trapping, the surface potential in the extrinsic region was measured by Koley *et al.* by using the Kelvin probe technique, and it was found that applying a high voltage in the OFF-state accumulates negative change on this surface [7].

It has been widely observed that the trapping in GaN HEMTs has a slow nature. Although fast components have also been reported [9], [10], the recovery time from current collapse is generally long ($>$ 100 s or even a few days) [6], [7], [11], [12]. This makes this phenomenon of critical relevance in every conceivable application of these devices, i.e., from RF systems to power electronics.

Trapping effects in GaN HEMTs are important for two reasons. First, they are a performance-limiting factor. In RF applications, for example, trapping results in limited RF performance, compared to what is expected from dc characterization [13]. As a result of their slow nature in the AlGaN/GaN system, traps also play a key role in reliability. As a device operates at high voltage, the electrons become trapped in various locations, degrading device performance. Moreover, it has been widely seen that the trapping effects increase after device degradation [11], [13]–[20]. The increased trapping reduces the performance of the device even more rapidly and thus undermines its reliability.

Various methods, such as deep-level transient spectroscopy (DLTS), gate-lag measurement, low-frequency noise measurement, and frequency-dependent g_m dispersion and conductance analysis, have been used in GaN HEMTs to study their trapping behavior [3], [15], [19], [21]–[23]. In spite of this, detailed understanding of the characteristics of the traps is still lacking today. In addition, the existing techniques are not easily incorporated in long-term electrical stress experiments.

In this paper, we present a methodology to analyze the trapping and detrapping behavior in GaN HEMTs that is amenable to integration with long-term stress experiments. Using the proposed technique, we determine the layer location, energy level, and trapping/detrapping time constants of the dominant traps that exist in the studied devices. This paper augments and refines the description of the methodology that is first introduced in [5]. In Section II, we describe the experimental setup and technical details of the proposed technique. In Section III, we present the results obtained in trapping and detrapping experiments on state-of-the-art GaN HEMTs. We summarize the key conclusions of this paper in Section IV.

II. Methodology

There are various methods to investigate the trapping behavior in semiconductor structures. However, these techniques are not always suitable for studying actual semiconductor devices

Manuscript received June 30, 2010; revised September 22, 2010; accepted October 8, 2010. Date of publication November 11, 2010; date of current version December 27, 2010. This work was supported in part by the Army Research Laboratory under Contract W911QX-05-C-0087 through the DARPA-WBGS Program and in part by the Office of Naval Research under Grant N00014-08-1-0655 through the DRIFT-MURI Program. The review of this paper was arranged by Editor A. Haque.

The authors are with the Microsystems Technology Laboratories, Massachusetts Institute of Technology, Cambridge, MA 02139 USA (e-mail: jungwoo@mit.edu).

Color versions of one or more of the figures in this paper are available online at http://ieeexplore.ieee.org.

Digital Object Identifier 10.1109/TED.2010.2087339

0018-9383/$26.00 © 2010 IEEE

due to their typically small dimensions. A good example is the DLTS [24]. Since the original technique relies on a measurement of capacitance, it is usually difficult to apply it to highly scaled transistors due to the difficulty in accurately measuring very small capacitance in a short time.

In order to overcome these difficulties, several techniques relying on current measurements have been developed. The gate-lag and drain-lag measurements [3], [9], [10] and drain current DLTS technique [25] are good examples of current-transient-based techniques that have been used in GaN FETs. In addition, frequency-dependent transconductance measurement and low-frequency noise measurement have been utilized to study the trapping behavior [21], [22], [26].

An additional difficulty arises when a trap characterization technique is desired to be integrated onto a comprehensive device characterization suite to study device degradation in real time, as is our case. For this to be possible, the trap characterization technique must be probe and cable compatible with the rest of the instrumentation, be very fast, and must yield useful information from single-temperature measurements. Toward this goal, in this paper, we have developed a new methodology to study the trapping behavior in GaN HEMT. In our preliminary studies, this technique was integrated in the middle of stress experiments to analyze the change in trapping behavior during high-voltage degradation [5], [27].

Our method consists of trapping and detrapping current-transient measurements and their analysis to obtain the corresponding time-constant spectra. As in other techniques based on current transients, we assume that the change in the current results from the change in trapping status in the device. We separately investigate the trapping and detrapping behavior. In the trapping experiments, a bias voltage is applied, and the drain and/or gate currents are sampled at certain points in a logarithmic time scale to monitor the carrier trapping. Different bias points are used in order to induce different modes of trapping and at different locations in the device. These bias points include the ON-state (high I_D and relatively high V_{DS}) and $V_{DS} = 0$ state (relatively high negative V_{GS} with $V_{DS} = 0$).

In the detrapping experiments, a trapping pulse in which both the drain and gate voltages are synchronously pulsed is first applied in order to induce carrier trapping. As in the trapping studies, we exploit various pulsing conditions (pulsewidth and voltage in ON-state and $V_{DS} = 0$ state for example) to induce different starting trapping situations at different locations. Right after removing the trapping pulse, we monitor the recovery transient of the current over a length of time. The transient data that emerges from these experiments is analyzed through a mathematical procedure that extracts the dominant time constants. This is described in detail in the following.

In our implementation, the current transient is measured through the sampling mode of an Agilent B1500A semiconductor parameter analyzer. In our system, the minimum time resolution is about 2 ms. Thus, the very first measurement of the current is performed 2 ms after voltage application. In the trapping experiments, the measurement is a simple sampling of the drain/gate bias current as a function of time.

In detrapping experiments, in principle, the maximum drain current $I_{D\max}$ is the most suitable parameter to monitor since

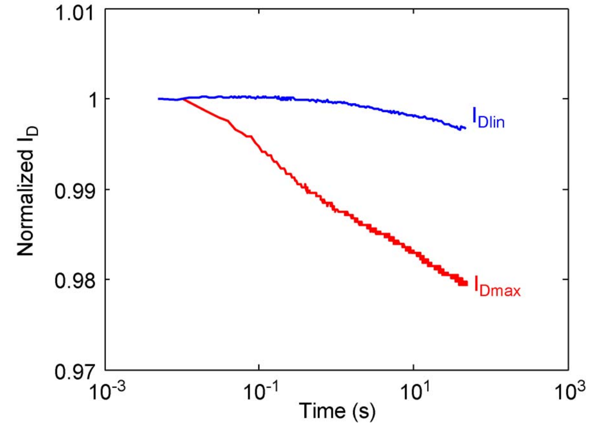

Fig. 1. Trapping transient of $I_{D\max}$ ($V_{GS} = 2$ V, $V_{DS} = 5$ V), and I_{Dlin} ($V_{GS} = 1$ V, $V_{DS} = 0.5$ V).

it is directly related to device performance. However, we find that the measurement of $I_{D\max}$ over an extended period of time induces a significant amount of trapping in itself due to the relatively high drain voltage that is used (> 5 V for typical GaN HEMTs). This is illustrated in Fig. 1, where we show the continuous measurements of $I_{D\max}$ (defined as $V_{GS} = 2$ V and $V_{DS} = 5$ V) over 50 s in a virgin device. A significant decrease in $I_{D\max}$ is observed. To overcome this difficulty, we instead measure the drain current in the linear regime, I_{Dlin} ($V_{GS} = 1$, $V_{DS} = 0.5$ V). Fig. 1 shows that a measurement of I_{Dlin} over a long period of time induces minimal trapping. This is due to the much lower V_{DG} and, thus, the electric field of the I_{Dlin} condition, as compared to the $I_{D\max}$ condition. In addition, because of large self-heating at the $I_{D\max}$ condition (~6 W/mm), it is difficult to accurately determine the device temperature when measuring $I_{D\max}$ to monitor the detrapping. This represents a significant drawback for understanding detrapping. In the measurement of I_{Dlin}, self-heating is negligible. Measuring I_{Dlin} is essentially identical to measuring R_{ON} $(= R_S + R_{\mathrm{CH}} + R_D)$, and we have already shown that $I_{D\max}$ and the series resistance show the same trapping and detrapping behavior [11].

In the detrapping experiments, the minimum time resolution of our instrumentation prevents us from measuring I_{Dlin} during the first 2 ms after removing the trapping pulse. As already shown in [12], this corresponds to about 40% of the current collapse in $I_{D\max}$ that we can measure with a much faster pulsed I–V system at room temperature. However, by lowering the temperature, we are able to obtain significant information because thermally activated detrapping processes become slower at lower temperatures.

The trapping and detrapping transient data, $I_{\mathrm{data}}(t)$, is analyzed by fitting them to a sum of pure exponentials in a least-mean-square fashion. The underlying assumption is that a current transient involves several independent trapping and detrapping processes, each decaying in time in an exponential way. This assumption makes sense for a detrapping process because a process of recovery from a nonequilibrium state of which decay rate is proportional to the population of the state follows exponentials time dependence. It also makes sense for a trapping process if the carriers have to overcome an energy barrier, as the rate of transport through the barrier is

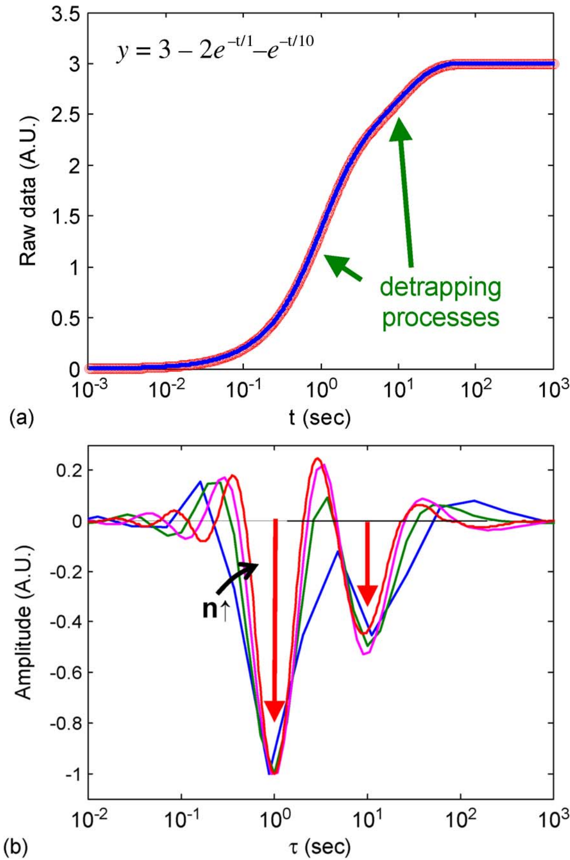

Fig. 2. Example of the time-constant analysis methodology. (a) Time-domain signal of an artificial current transient (red: data, blue: fitted curve). (b) Time-constant spectrum extracted from the fitting of the time-domain signal with various numbers of exponentials ($n = 20, 50, 100, 500$).

proportional to the carrier population. The fitting function can be expressed as

$$I_{\text{fitted}} = \sum_{i=1}^{n} a_i \exp(-t/\tau_i) + I_{\infty}. \qquad (1)$$

The fitting is performed to minimize the sum of $|I_{\text{data}} - I_{\text{fitted}}|^2$ at the measured points. In this process, a_i's are the fitting parameters to be evaluated, whereas τ_i's are the predefined constants. For the fitting function, we typically use 100 exponentials with time constants τ_i that are equally spaced logarithmically in time. Positive (negative) values of a_i correspond to the trapping (detrapping) processes. a_i represents the magnitude of the trapping (detrapping) process of time constant τ_i. Our measurement and analysis are carried out in the 10^{-3} to 10^3 s range. After the fitting is done, the extracted values of a_i can be used to construct a *time-constant spectrum* by plotting them as a function of τ_i.

In order to show how this methodology works, we apply our fitting algorithm to an artificial data set. This is illustrated in Fig. 2. The time-domain signal in this example consists of two pure exponential detrapping components with time constants of 1 and 10 s. In this unitless example, the amplitudes of the two components are 2 and 1, respectively. After we generate the data, we fit it using (1) with various numbers of exponentials ($n = 20$, 50, 100, and 500), and we then plot the obtained amplitudes in the time-constant spectrum in Fig. 2(b). This clearly reveals the two components with their correct time constants and correct relative amplitudes. As n increases, the time constants and amplitudes become more accurate, although, even with $n = 20$, the maximum errors in the time constant and amplitude are 11% and 5%, respectively.

Although two delta-function-like peaks at 1 and 10 s would be an ideal representation of the transient of Fig. 2(a) in the time-constant domain, the method yields two peaks with finite width. In addition, a few small ripples appear around the two peaks. These nonidealities are caused by two reasons. First, we used a finite number of exponential components for the fitting in (1). Using more exponentials can reduce the width of the peaks to some extent, as shown in Fig. 2(b), but at the cost of more computing time for the fitting process. Since linewidth does not significantly improve beyond $n = 100$, we have selected this number of points for our paper. Second, although the basis functions—the decaying exponentials—in (1) make physical sense, as previously mentioned, they are not orthogonal to one another. In fact, this is why we cannot do a simpler analysis, e.g., something that is similar to a Fourier transform, and also, there is a need for a least-mean-square fitting approach. Because of these reasons, in our paper, we regard any peak with full-width at half-maximum of 0.65 dec (for $n = 100$) as a pure exponential process, as shown in Fig. 2.

In principle, this fitting is a linear optimization problem. However, in order to prevent over-fitting that would make the time-constant spectrum extremely noisy, a few constraints such as lower and upper bounds or smoothness in the spectrum have been added. In the latter case, for example, $|a_i - a_{i+i}|^2$ terms have been added to the optimization cost function. Another approach could be also minimizing $|a_i|$'s. Due to these constraints, this problem mathematically turns into a nonlinear optimization, and it takes quite a long time to be solved. As a result, we have limited the number of exponentials to 100, which, in our experience, represents a good compromise between computation time and physical meaningfulness of the result.

Our methodology has several advantages over conventional trap analysis methods. First, by using a double pulse where both the drain and gate voltages can be simultaneously pulsed between two arbitrary bias points, we can induce various states of trapping in different regions of the device. This allows us to spatially localize traps, as will be shown later. Second, the extraction of a *time-constant spectrum* is particularly powerful when multiple processes are simultaneously present. As the example in Fig. 2 illustrates, our technique is capable of separating individual processes with their well-defined time constants and relative amplitude just as in the DLTS method.

III. RESULTS

Transient experiments in unstressed GaN HEMTs biased in different ways have been performed at chuck temperatures between −60 °C and 130 °C. In order not to degrade the device during the experiments, the maximum voltage is kept below 10 V in all cases. This voltage is well below the critical voltage beyond which trapping behavior in the device has been observed to significantly increase in this kind of transistors [5],

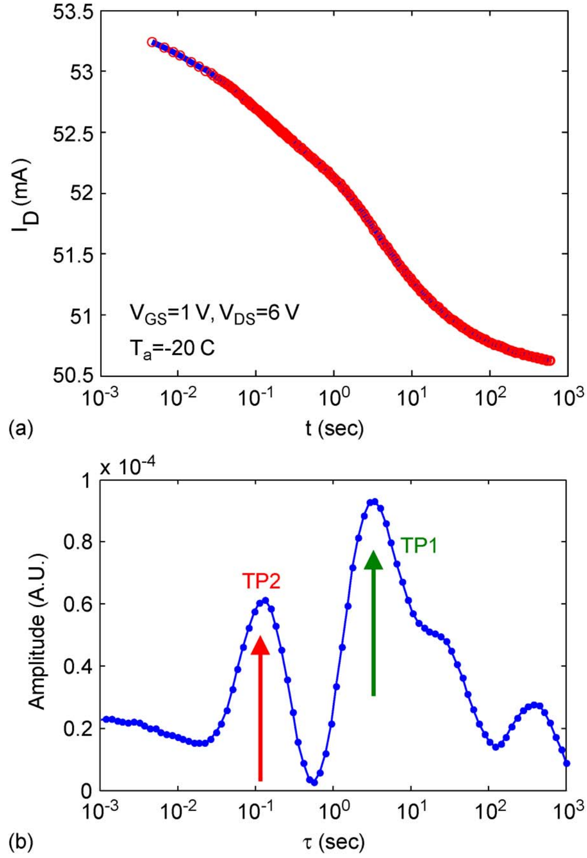

Fig. 3. (a) Trapping transient of I_D and (b) the corresponding time-constant spectrum of a GaN HEMT in the ON-state ($V_{GS} = 1$ V, $V_{DS} = 6$ V) at 30 °C. No pulse is applied before the transient measurement. Two major trapping processes, i.e., TP1 and TP2, can be identified.

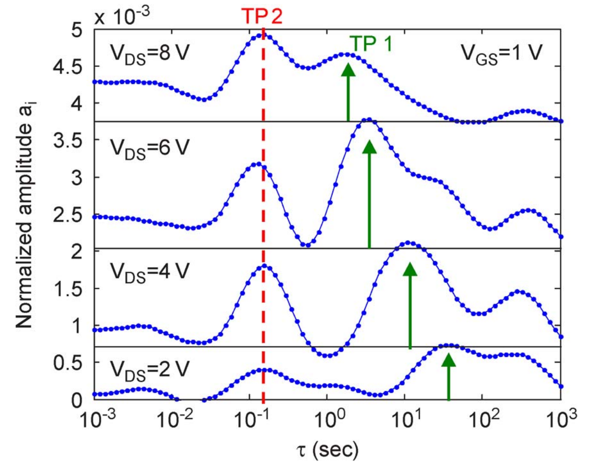

Fig. 4. Time-constant spectrum for trapping transients in the ON-state with $V_{GS} = 1$ V and different $V_{DS} = 2 - 8$ V at 30 °C. TP1 is affected by V_{DS}, whereas TP2 is not.

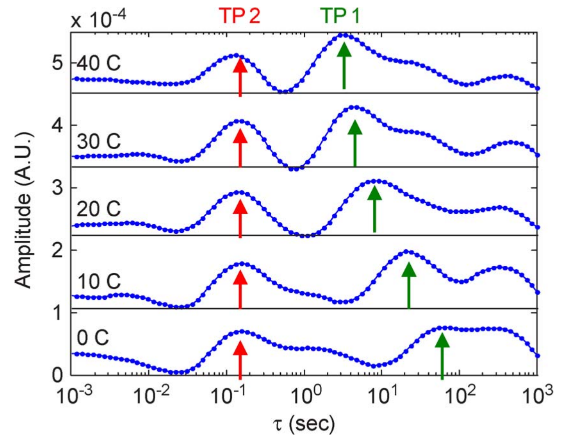

Fig. 5. Time-constant spectrum for trapping transients in the ON-state with $V_{GS} = 1$ V and $V_{DS} = 6$ V at different temperatures. The temperature is changed from 0 °C to 40 °C. TP1 is affected by temperature, whereas TP2 is not.

[28]. After each transient measurement, the initial condition of the device was completely recovered by shining microscope light for 30 s. In this way, all trapped electrons are detrapped. In general, although visible light works in many cases, ultraviolet light is preferable for detrapping purposes, particularly if deep levels are present. All the experiments in this section have been performed on the same device, but they are representative of the results obtained on many other devices.

A. Trapping Behavior

First, we study the trapping behavior of a device in the ON-state. The bias is $V_{GS} = 1$ V and $V_{DS} = 2$ to 8 V. We monitor only I_D for fast measurement and better signal-to-noise ratio. A typical I_D transient at $V_{DS} = 6$ V at 30 °C is shown in Fig. 3. The corresponding time-constant spectrum is also shown. As it can be seen, I_D decreases over time in a transient that persists even after 10 min. This reduction in I_D is fully recoverable after microscope light illumination, suggesting it is solely due to temporary trapping in traps that exist in the virgin device.

In the time-constant spectrum, two major trapping processes, which we label TP1 and TP2, can be identified. At this temperature, the time constants of these processes are about 3 and 0.1 s, respectively. In similar experiments in which different values of V_{DS} are applied, we find that the time constant of TP2 does not change, although its amplitude increases with V_{DS} (see Fig. 4). On the other hand, the time constant of TP1 is reduced as V_{DS} is increased. This can result from either higher temperature due to high power dissipation or could be a consequence of the higher electric field at high V_{DS}. This is clarified through the subsequent experiments.

In order to understand the temperature dependence of the trapping behavior in the ON-state, we have performed the same experiment as in Fig. 3 at different temperatures. Fig. 5 shows the time-constant spectrum of the trapping transients. We find that the time constant for TP1 is thermally activated, whereas that for TP2 is insensitive to temperature. This suggests that, in trapping process TP1, the electrons have to overcome an energy barrier before they can get trapped. Additionally, for TP1, the linewidth of the peak is broader than the intrinsic linewidth [see Fig. 2(b)], suggesting a broad-trap-energy distribution or thermal broadening. From the time constant of TP1 at different temperatures and voltages, its activation energy is estimated to be between 0.62 and 0.90 eV. The relatively large variation in E_a is mainly due to uncertainty in the device thermal resistance and, therefore, its temperature. In the ON-state, the temperature in the device can significantly increase due to high power

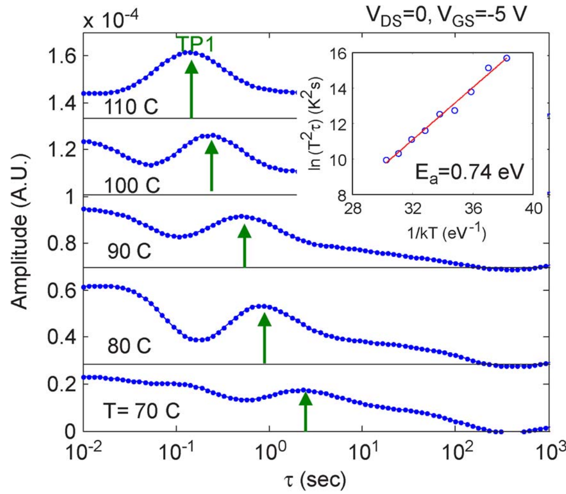

Fig. 6. Time-constant spectrum for the trapping transients of I_G in the $V_{DS} = 0$ state with $V_{GS} = -5$ V at different temperatures (70 °C–110 °C). (Inset) Arrhenius plot of the time constant is shown ($E_a = 0.74$ eV).

dissipation. Although the channel temperature can be calculated or measured through various methods [29]–[31], it is difficult to precisely estimate the temperature at the exact region where this trapping process occurs. As a result, experiments where no self-heating occurs are preferred to extract E_a.

To resolve these issues, we have performed similar trapping experiments in the $V_{DS} = 0$ state where device self-heating is negligible. In this case, a negative gate bias of −5 V is applied, and I_G is monitored over time (the channel current is zero). Typical time-constant spectra for different temperatures are shown in Fig. 6. As in the ON-state, in this experiment, we observe a temperature-dependent process. The time constant of this process is close to that of TP1 in the ON-state with $V_{DG} = 5$ V, when one takes into consideration the self-heating that is present in the ON-state. Additionally, the activation of the time constant is 0.74 eV, which is within the range of E_a that we observe in the ON-state experiments. This suggests that the trapping process that we observe in the $V_{DS} = 0$ state in Fig. 6 is the same process as TP1 in the ON-state in Figs. 3–5. Interestingly, the time constant and E_a of TP1 in the $V_{DS} = 0$ state are independent of the V_{GS} value (not shown). This is consistent with our interpretation that the V_{DS} dependence of the time constant of TP1 in the ON-state arises from self-heating.

Unlike the ON-state, in the $V_{DS} = 0$ state, we do not observe a TP2-like process that is temperature independent. Since all the trapping in the $V_{DS} = 0$ state should result from gate leakage current, we can then conclude that TP1 is associated with electron injection from the gate and trapping either inside the AlGaN barrier or at the surface close to the gate. However, the extended features that are visible in Fig. 6 suggest the existence of a broad range of trapping processes where TP1 is the only the most prominent. On the other hand, since TP2 appears only when the channel current is present, it should then be related to the trapping of channel electrons perhaps through a tunneling process. We have ruled out a thermal transient origin for TP2 due to self-heating because this process is much slower (∼0.1 s) than the typical thermal time constant ($\sim \mu$s). In addition, the fact that the time constant of TP2 does not change with temperature (see Fig. 5) is also inconsistent with a purely thermal origin as the thermal conductivity changes with temperature [32]–[34], and this would lead to a thermal time constant that would also depend on temperature. The fact that TP2 is observed at as low a voltage as $V_{DG} = 1$ V (see Fig. 4) suggests that it is unlikely to be a hot-electron trapping process at the surface or inside the AlGaN. Hot-electron-related processes should have a negative temperature dependence and an exponential dependence on V_{DG}. Neither does TP2 exponentially decay with V_{DG} (see Fig. 4) nor it shows a negative temperature dependence (see Fig. 5). As a result, we believe that this process occurs in the channel or in the buffer region.

A pictorial view of trapping processes TP1 and TP2 is shown in Fig. 7. In the ON-state, the gate current injects electrons into AlGaN and the surface, and some of these electrons are trapped in this region (TP1). Some of the channel electrons are captured by the traps in the channel or in the buffer (TP2). On the other hand, in the $V_{DS} = 0$ state, only the first process (TP1) occurs in both the source and drain sides.

B. Detrapping Behavior

We have also examined the recovery processes after the application of a pulse that leads to electron trapping. This section shows the results obtained on the very same device as in the previous section. They are representative of many devices that we have studied.

Fig. 8 shows a detrapping transient of I_{Dlin} and the corresponding time-constant spectrum at −20 °C, right after trapping is induced by applying a 1-s-long $V_{DS} = 0$ state pulse of $V_{GS} = -10$ V. As one can see, at 2 ms, this pulse introduced a current collapse of about 1.3% in I_{Dlin}. Up to around 1 s, the collapsed drain current does not recover. For longer times, the current recovers through a well-defined detrapping process, which is marked as DP1, with a time constant $\tau \sim 4$ s. As shown in Fig. 9, this time constant depends on temperature and is thermally activated with a very well defined activation energy $E_a = 0.57$ eV. A trap at around this energy level with respect to the conduction band edge of the AlGaN is widely observed in DLTS and other transient techniques [21], [25], [35], [36]. This kind of trap was found to increase after device degradation [5], [21], [35], [36]. Since, in the $V_{DS} = 0$ condition, we know that trapping only occurs in the AlGaN barrier or at the surface close to the gate (TP1 in Fig. 7), it is reasonable to conclude that detrapping process DP1 that is observed here is a reverse process of those trapping processes, including TP1. This is schematically shown in Fig. 10. Interestingly, the sum of the activation energy of TP1 (0.74 eV) and DP1 (0.57 eV) is close to the Schottky barrier height (1.27 eV) [37]. This suggests that this trap is inside the AlGaN barrier and is generally consistent with the overall picture in Figs. 7 and 10. Tapajna *et al.* also concluded that a trap with a similar behavior is located in the AlGaN barrier [36].

Fig. 11 shows a recovery transient after electron trapping induced by an ON-state pulse (1 s, $V_{GS} = 0$ V, $V_{DS} = 10$ V). In this condition, we know that during the trapping pulse, high drain current flows, and the trapping takes place inside the AlGaN or at the surface close to the gate edge (TP1) and most

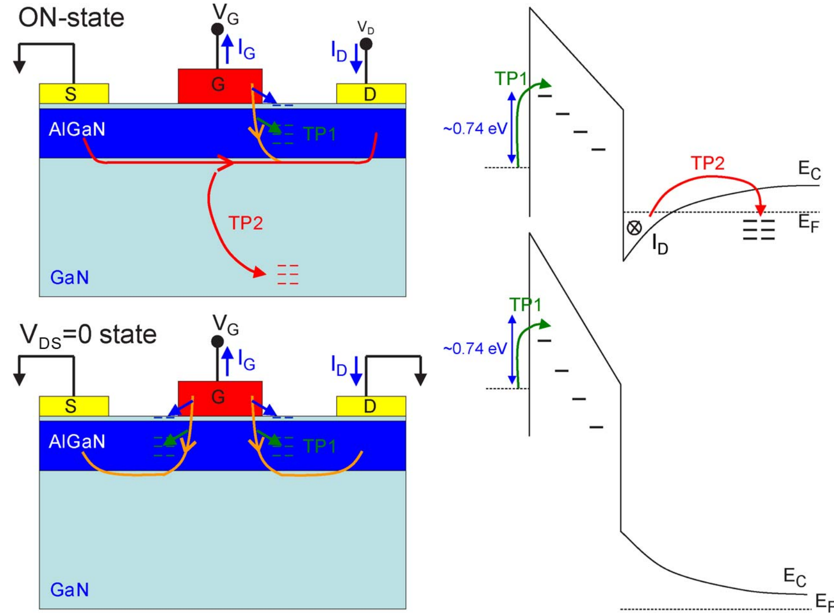

Fig. 7. Schematic diagrams of the trapping behavior in the ON-state and $V_{DS} = 0$ state. Corresponding band diagrams are also shown. Arrows indicate the electron flow.

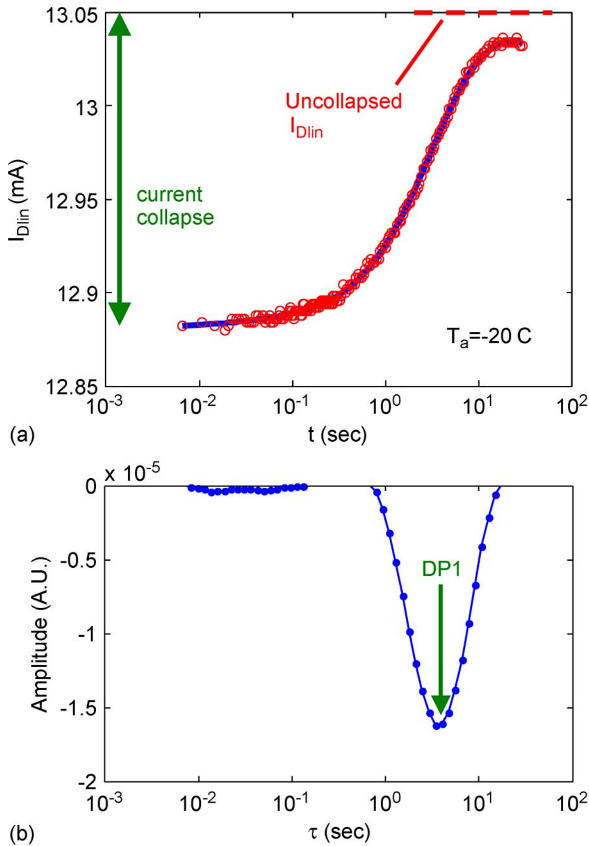

Fig. 8. (a) Recovery transient of $I_{\rm Dlin}$ and (b) corresponding time-constant spectrum at -20 °C after applying a 1-s $V_{DS} = 0$ and $V_{GS} = -10$ V trapping pulses.

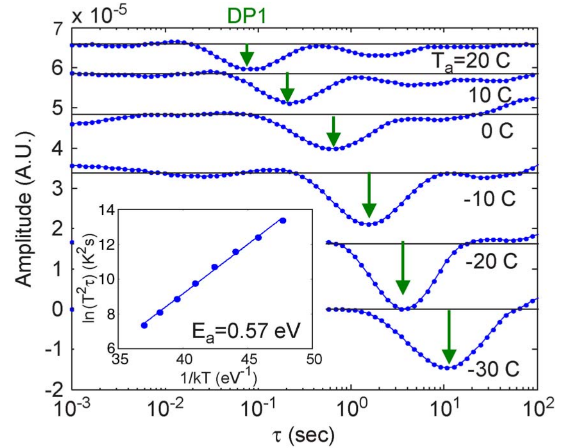

Fig. 9. Time-constant spectra of the detrapping transients after 1-s $V_{DS} = 0$ and $V_{GS} = -10$ V pulses for $T = -30$ °C to 20 °C. (Inset) Time constant of DP1 as a function of temperature. $E_a = 0.57$ eV.

likely in the buffer (TP2). During the detrapping, we observe two distinct time constants, which are labeled as DP1 ($\tau \sim$ 4 s) and DP2 ($\tau \sim 0.1$ s). Through the temperature-dependent experiments between -30 °C and 100 °C (not shown), we have observed that DP1 exhibits the same time constant and temperature dependence ($E_a = 0.57$ eV) as in the $V_{DS} = 0$ state. On the other hand, DP2 is temperature independent. This suggests that DP1, after the ON-state pulse, results from the same trap that is involved in DP1 for the $V_{DS} = 0$ state pulse and that DP2 involves a bottleneck transport process in series with a detrapping process that is itself much faster than 0.1 s. This is in perfect symmetry with the experimental observations on TP2 in the earlier section.

In order to further explore the physics of DP1 and DP2, we have investigated the dependence of these two detrapping peaks on the parameters of the trapping pulse (time duration, current, and voltage). The trapping pulsewidth dependence is shown in Fig. 12. DP2 is found to be negligible for an ON-state pulse that is shorter than 0.1 s. This coincides with the value of the time constant of TP2 obtained in trapping experiments (see previous section), which was attributed to the trapping of the channel electrons in the buffer or channel area. It further

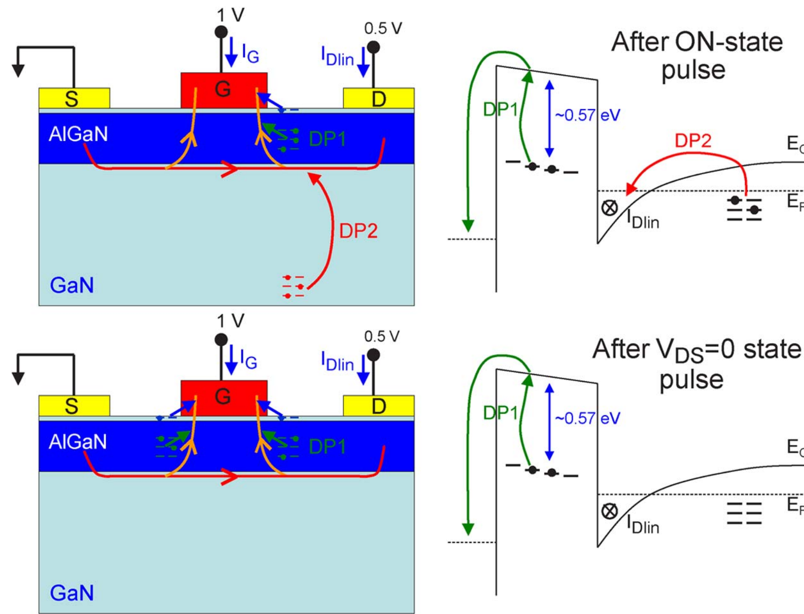

Fig. 10. Schematic diagrams of the detrapping behavior after the current collapse induced by (top) an ON-state and (bottom) a $V_{DS} = 0$ state pulse. Corresponding band diagrams for the detrapping processes are also shown. Arrows indicate the electron flow.

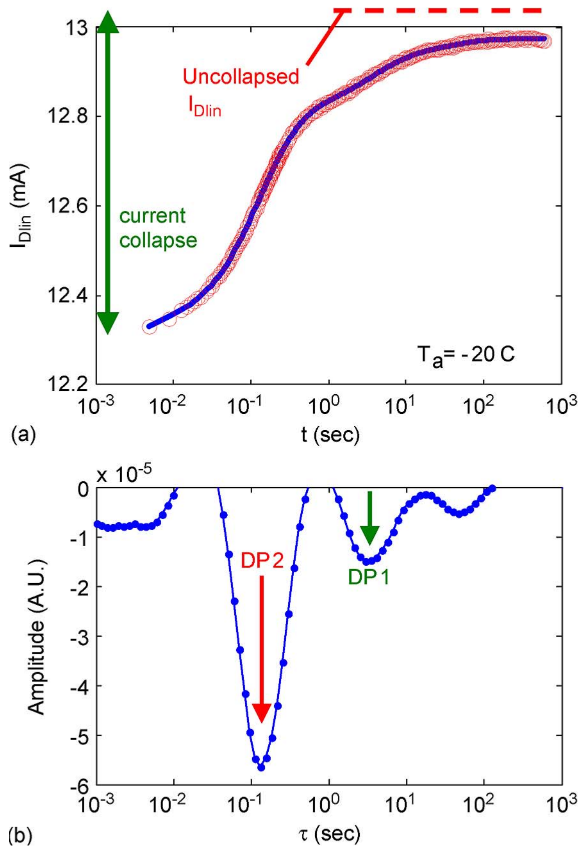

Fig. 11. (a) Time evolution of I_{Dlin} and (b) corresponding time-constant spectrum at −20 °C for 10 min after applying 1-s $V_{DS} = 10$ and $V_{GS} = 0$ V pulses.

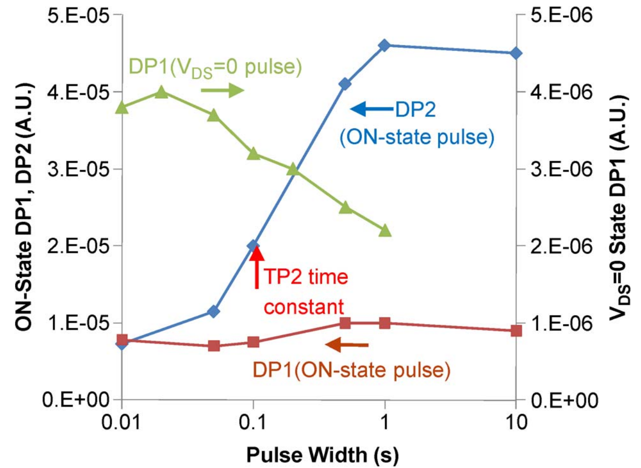

Fig. 12. Trapping pulsewidth dependence of DP1 and DP2 for ON-state pulse ($V_{DS} = 10$ V) and DP1 for $V_{DS} = 0$ state pulse ($V_{GS} = -10$ V).

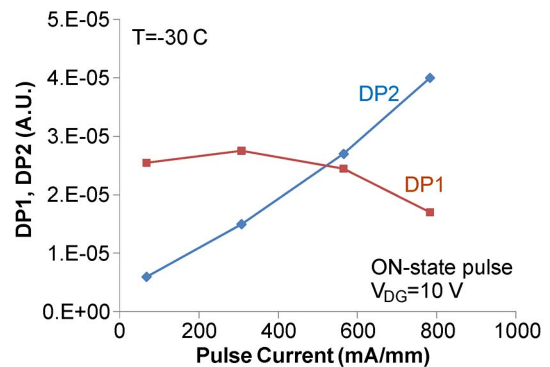

Fig. 13. Trapping pulse current dependence of DP1 and DP2 after 1-s ON-state pulse at −30 °C.

suggests that TP2 and DP2 are the exact inverse processes of each other, engaging the very same set of traps because the trapping pulses that are shorter than the time constant of TP2 will not introduce the trapping to those traps. On the other hand, DP1 for the ON-state pulse does not show this kind of threshold in the pulsewidth, consistent with the observations in [36]. In contrast with this, DP1, after the $V_{\mathrm{DS}} = 0$ pulse, decreases as the pulsewidth increases. This may be due to the fact that the

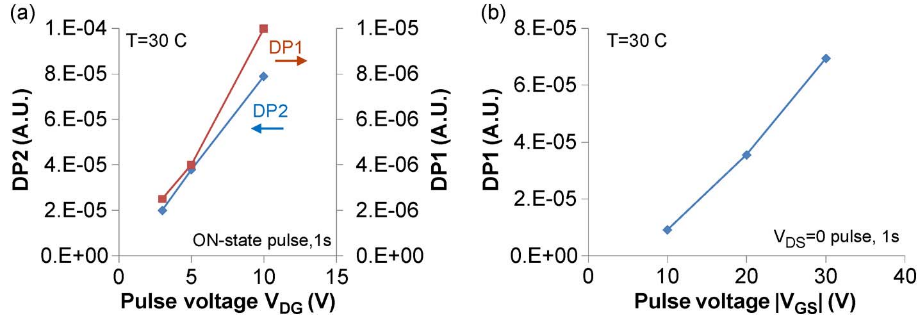

Fig. 14. Amplitude of the detrapping processes as a function of the voltage of the trapping pulse. (a) ON-state trapping pulse and (b) $V_{DS} = 0$ state trapping pulse.

electric field at the gate corner is reduced due to the trapping itself [8], [38]. As a result, some of the trapped electrons get detrapped as the trapping time increases (increasing pulsewidth), and the electric field decreases.

We have also investigated the impact of the current that flows through the device during the trapping pulse on the magnitude of the detrapping processes. Fig. 13 shows that the magnitude of DP2 scales with the current level of the trapping pulse at constant $V_{DG} = 10$ V and roughly goes to zero when the current goes to zero. This is consistent with the previous finding that in the $V_{DS} = 0$ state, neither TP2 nor DP2 is present as the channel current is zero and confirms the channel or buffer nature of these transients. Since the time constant of DP2 after the ON-state pulse is always exactly the same as that of TP2 observed in the ON-state trapping process (see Figs. 3–5 and 11), these results strongly suggest that DP2 and TP2 are the inverse processes of each other and that both are related to the buffer trapping/detrapping of the channel electrons (see Figs. 7 and 10). The time constant ($\sim$0.1 s) is the RC charging/discharging time [39] or the transit time that it takes for an electron to reach the traps that are deep in the buffer. In fact, Binari *et al.* ascribed the current collapse induced by a high current and a high V_{DS} pulse to the trapping in the buffer [3], which is consistent with our result. A pictorial diagram of DP2 process is shown in Fig. 10. On the other hand, DP1 is almost constant over the pulse current, except that it slightly decreases at very high current. This may be due to the reduction of the electric field at the gate corner as the channel fully opens. In addition, the channel temperature becomes higher at high current, resulting in less trapping. The fact that DP1 does not increase with I_D confirms that the source of electrons for DP1 is not the channel but the leakage from the gate.

Finally, we have examined the voltage dependence. This is shown in Fig. 14. As it can be seen, the magnitudes of both DP1 and DP2 linearly increase with V_{DG} of the ON-state pulse [see Fig. 14(a)]. This linear dependence of DP2 again shows that DP2 is not related to hot-electron trapping that should exhibit the exponential dependence on V_{DG}. The same linear behavior with $|V_{GS}|$ is observed for the amplitude of DP1 after the $V_{DS} = 0$ pulse [see Fig. 14(b)].

IV. CONCLUSION

We have presented a simple current-transient methodology to investigate the characteristics of the traps in GaN HEMTs. The method consists of the measurement of the trapping and detrapping transients and the analysis of the data in time-constant domain. We have identified several traps located above the channel, in the AlGaN or at the surface, and in the buffer. Under ON-state bias, where both high electric field under the gate edge and high current in the channel are present, the trapping takes place in two distinct regions: the AlGaN barrier (or surface) and the buffer (or channel). The trapping in the AlGaN is thermally activated, whereas the buffer trapping is temperature independent. On the other hand, under $V_{DS} = 0$ state with negative gate bias, only the trapping to AlGaN takes place due to lack of channel current.

In the recovery transients, we have identified several detrapping processes. The detrapping from the AlGaN barrier has been found to be thermally activated, but the detrapping from the buffer did not show any temperature dependence. The latter process has been found to be the exact inverse process of the buffer trapping process in the ON-state.

Because our methodology is amenable to integration with long-term electrical reliability experiments [5], [36], we expect this technique to be used for understanding the evolution of trapping behavior as a result of electrical degradation in GaN HEMTs and other electronic devices.

ACKNOWLEDGMENT

The authors would like to acknowledge collaboration with TriQuint Semiconductor. This research has taken place in part at the Microsystems Technology Laboratories, Massachusetts Institute of Technology.

REFERENCES

[1] Y. F. Wu, M. Moore, A. Abrahamsen, M. Jacob-Mitos, P. Parikh, S. Heikman, and A. Burk, “High-voltage millimeter-wave GaN HEMTs with 13.7 W/mm power density,” in *IEDM Tech. Dig.*, 2007, pp. 405–407.

[2] Y. Uemoto, D. Shibata, M. Yanagihara, H. Ishida, H. Matsuo, S. Nagai, N. Batta, M. Li, T. Ueda, T. Tanaka, and D. Ueda, “8300 V blocking voltage AlGaN/GaN power HFET with thick poly-AlN passivation,” in *IEDM Tech. Dig.*, 2007, pp. 861–864.

[3] S. C. Binari, P. B. Klein, and T. E. Kazior, “Trapping effects in GaN and SiC microwave FETs,” *Proc. IEEE*, vol. 90, no. 6, pp. 1048–1058, Jun. 2002.

[4] H. Kim, V. Tilak, B. M. Green, J. A. Smart, W. J. Schaff, J. R. Shealy, and L. F. Eastman, “Reliability evaluation of high power AlGaN/GaN HEMTs on SiC substrate,” *Phys. Stat. Sol. (A)*, vol. 188, no. 1, pp. 203–206, Nov. 2001.

[5] J. Joh and J. A. del Alamo, “Impact of electrical degradation on trapping characteristics of GaN high electron mobility transistors,” in *IEDM Tech. Dig.*, 2008, pp. 461–464.

[6] R. Vetury, N. Q. Zhang, S. Keller, and U. K. Mishra, “The impact of surface states on the DC and RF characteristics of AlGaN/GaN HFETs,” *IEEE Trans. Electron Devices*, vol. 48, no. 3, pp. 560–566, Mar. 2001.

[7] G. Koley, V. Tilak, L. F. Eastman, and M. G. Spencer, “Slow transients observed in AlGaN/GaN HFETs: Effects of SiN_x passivation and UV illumination,” *IEEE Trans. Electron Devices*, vol. 50, no. 4, pp. 886–893, Apr. 2003.

[8] R. J. Trew, D. S. Green, and J. B. Shealy, “AlGaN/GaN HFET reliability,” *IEEE Microw. Mag.*, vol. 10, no. 4, pp. 116–127, Jun. 2009.

[9] G. Meneghesso, G. Verzellesi, R. Pierobon, F. Rampazzo, A. Chini, U. K. Mishra, C. Canali, and E. Zanoni, “Surface-related drain current dispersion effects in AlGaN-GaN HEMTs,” *IEEE Trans. Electron Devices*, vol. 51, no. 10, pp. 1554–1561, Oct. 2004.

[10] J. M. Tirado, J. L. Sanchez-Rojas, and J. I. Izpura, “Trapping effects in the transient response of AlGaN/GaN HEMT devices,” *IEEE Trans. Electron Devices*, vol. 54, no. 3, pp. 410–417, Mar. 2007.

[11] J. Joh and J. A. del Alamo, “Mechanisms for electrical degradation of GaN high-electron mobility transistors,” in *IEDM Tech. Dig.*, 2006, pp. 415–418.

[12] J. Joh, J. A. del Alamo, and J. Jimenez, “A simple current collapse measurement technique for GaN high-electron mobility transistors,” *IEEE Electron Device Lett.*, vol. 29, no. 7, pp. 665–667, Jul. 2008.

[13] D. Pavlidis, P. Valizadeh, and S. H. Hsu, “AlGaN/GaN high electron mobility transistor (HEMT) reliability,” in *Proc. GaAs Symp.*, 2005, pp. 265–268.

[14] J. A. Mittereder, S. C. Binari, P. B. Klein, J. A. Roussos, D. S. Katzer, D. F. Storm, D. D. Koleske, A. E. Wickenden, and R. L. Henry, “Current collapse induced in AlGaN/GaN high-electron-mobility transistors by bias stress,” *Appl. Phys. Lett.*, vol. 83, no. 8, pp. 1650–1652, Aug. 2003.

[15] T. Mizutani, Y. Ohno, M. Akita, S. Kishimoto, and K. Maezawa, “A study on current collapse in AlGaN/GaN HEMTs induced by bias stress,” *IEEE Trans. Electron Devices*, vol. 50, no. 10, pp. 2015–2020, Oct. 2003.

[16] H. Kim, R. M. Thompson, V. Tilak, T. R. Prunty, J. R. Shealy, and L. Eastman, “Effects of SiN passivation and high-electric field on AlGaN-GaN HFET degradation,” *IEEE Electron Device Lett.*, vol. 24, no. 7, pp. 421–423, Jul. 2003.

[17] A. P. Zhang, E. B. Kaminsky, A. F. Allen, J. W. Hedrick, A. Vertiatchikh, and L. F. Eastman, “Stability of AlGaN/GaN high-power HEMTs under DC and RF stresses,” *Electron. Lett.*, vol. 40, no. 19, pp. 1229–1230, Sep. 2004.

[18] A. M. Conway, M. Chen, P. Hashimoto, P. J. Willadsen, and M. Micovic, “Accelerated RF life testing of GaN HFETs,” in *Proc. IEEE IRPS*, 2007, pp. 472–475.

[19] G. Meneghesso, G. Verzellesi, F. Danesin, F. Rampazzo, F. Zanon, A. Tazzoli, M. Meneghini, and E. Zanoni, “Reliability of GaN high-electron-mobility transistors: State of the art and perspectives,” *IEEE Trans. Device Mater. Rel.*, vol. 8, no. 2, pp. 332–343, Jun. 2008.

[20] J. A. del Alamo and J. Joh, “GaN HEMT reliability,” *Microelectron. Reliab.*, vol. 49, no. 5, pp. 1200–1206, 2009.

[21] A. Sozza, C. Dua, E. Morvan, M. A. diForte-Poisson, S. Delage, F. Rampazzo, A. Tazzoli, F. Danesin, G. Meneghesso, E. Zanoni, A. Curutchet, N. Malbert, N. Labat, B. Grimbert, and J.-C. De Jaeger, “Evidence of traps creation in GaN/AlGaN/GaN HEMTs after a 3000 hour on-state and off-state hot-electron stress,” in *IEDM Tech. Dig.*, 2005, pp. 590–593.

[22] P. Valizadeh and D. Pavlidis, “Effects of RF and DC stress on AlGaN/GaN MODFETs: A low-frequency noise-based investigation,” *IEEE Trans. Device Mater. Rel.*, vol. 5, no. 3, pp. 555–563, Sep. 2005.

[23] R. Stoklas, D. Gregusova, J. Novak, A. Vescan, and P. Kordos, “Investigation of trapping effects in AlGaN/GaN/Si field-effect transistors by frequency dependent capacitance and conductance analysis,” *Appl. Phys. Lett.*, vol. 93, no. 12, p. 124 103, Sep. 2008.

[24] D. V. Lang, “Deep–level transient spectroscopy: A new method to characterize traps in semiconductors,” *J. Appl. Phys.*, vol. 45, no. 7, pp. 3023–3032, Jul. 1974.

[25] T. Mizutani, T. Okino, K. Kawada, Y. Ohno, S. Kishimoto, and K. Mzezawa, “Drain current DLTS of AlGaN/GaN HEMTs,” *Phys. Stat. Sol. (A)*, vol. 200, no. 1, pp. 195–198, Nov. 2003.

[26] P. Valizadeh and D. Pavlidis, “Investigation of the impact of Al mole-fraction on the consequences of RF stress on $Al_xGa_{1-x}N$/GaN MODFETs,” *IEEE Trans. Electron Devices*, vol. 52, no. 9, pp. 1933–1939, Sep. 2005.

[27] J. Joh and J. A. del Alamo, “Trapping vs. permanent degradation in GaN high electron mobility transistors,” in *Proc. ICNS*, 2009, pp. 947–948.

[28] J. Joh and J. A. del Alamo, “Critical voltage for electrical degradation of GaN high-electron mobility transistors,” *IEEE Electron Device Lett.*, vol. 29, no. 4, pp. 287–289, Apr. 2008.

[29] A. M. Darwish, A. J. Bayba, and H. A. Hung, “Thermal resistance calculation of AlGaN-GaN devices,” *IEEE Trans. Microw. Theory Tech.*, vol. 52, no. 11, pp. 2611–2620, Nov. 2004.

[30] J. Joh, U. Chowdhury, T. M. Chou, H. Q. Tserng, and J. L. Jimenez, “Method for estimation of the channel temperature of GaN high electron mobility transistors,” in *Proc. ROCS Workshop*, 2007, pp. 87–89.

[31] A. Sarua, H. Ji, M. Kuball, M. J. Uren, T. Martin, K. P. Hilton, and R. S. Balmer, “Integrated micro-Raman/infrared thermography probe for monitoring self-heating in AlGaN/GaN transistor structures,” *IEEE Trans. Electron Devices*, vol. 53, no. 10, pp. 2438–2447, Oct. 2006.

[32] A. Jezowski, B. A. Danilchenko, M. Bockowski, I. Grzegory, S. Krukowski, T. Suski, and T. Paszkiewicz, “Thermal conductivity of GaN crystals in 4.2–300 K range,” *Solid State Commun.*, vol. 128, no. 2/3, pp. 69–73, Oct. 2003.

[33] J. Zou, D. Kotchetkov, A. A. Balandin, D. I. Florescu, and F. H. Pollak, “Thermal conductivity of GaN films: Effects of impurities and dislocations,” *J. Appl. Phys.*, vol. 92, no. 5, pp. 2534–2539, Sep. 2002.

[34] G. A. Slack, “Thermal conductivity of pure and impure silicon, silicon carbide, and diamond,” *J. Appl. Phys.*, vol. 35, no. 12, pp. 3460–3466, 1964.

[35] A. Chini, F. Fantini, V. Di Lecce, M. Esposto, A. Stocco, N. Ronchi, F. Zanon, G. Meneghesso, and E. Zanoni, “Correlation between DC and rf degradation due to deep levels in AlGaN/GaN HEMTs,” in *IEDM Tech. Dig.*, 2009, pp. 1–4.

[36] M. Tapajna, R. J. T. Simms, Y. Pei, U. K. Mishra, and M. Kuball, “Integrated optical and electrical analysis: Identifying location and properties of traps in AlGaN/GaN HEMTs during electrical stress,” *IEEE Electron Device Lett.*, vol. 31, no. 7, pp. 662–664, Jul. 2010.

[37] Z. Lin, W. Lu, J. Lee, D. Liu, J. S. Flynn, and G. R. Brandes, “Barrier heights of Schottky contacts on strained AlGaN/GaN heterostructures: Determination and effect of metal work functions,” *Appl. Phys. Lett.*, vol. 82, no. 24, pp. 4364–4366, Jun. 2003.

[38] S. Demirtas and J. A. del Alamo, “Effect of trapping on the critical voltage for degradation in GaN high electron mobility transistors,” in *Proc. IEEE IRPS*, 2010, pp. 134–138.

[39] E. Kohn, I. Daumiller, M. Kunze, M. Neuburger, M. Seyboth, T. J. Jenkins, J. S. Sewell, J. Van Norstand, Y. Smorchkova, and U. K. Mishra, “Transient characteristics of GaN-based heterostructure field-effect transistors,” *IEEE Trans. Microw. Theory Tech.*, vol. 51, no. 2, pp. 634–642, Feb. 2003.

Jungwoo Joh received the B.S. degree from Seoul National University, Seoul, Korea, in 2002 and the M.S. and Ph.D. degrees from Massachusetts Institute of Technology, Cambridge, MA, in 2007 and 2009, respectively, all in electrical engineering.

From 2002 to 2005, he was with Alticast, Seoul, Korea, as a Software Engineer. Since 2005, he has been conducting research on reliability, modeling, and characterization of GaN HEMTs with Microsystems Technology Laboratories, Massachusetts Institute of Technology.

Jesús A. del Alamo received the Telecommunications Engineer degree from the Polytechnic University of Madrid, Madrid, Spain, in 1980 and the M.S. and Ph.D. degrees in electrical engineering from Stanford University, Stanford, CA, in 1983 and 1985, respectively.

From 1985 to 1988, he was with NTT LSI Laboratories, Atsugi, Japan, and since 1988, he has been with the Department of Electrical Engineering and Computer Science, Massachusetts Institute of Technology, where he is currently a Donner Professor and MacVicar Faculty Fellow. His current research interests are microelectronics technologies for communications and logic processing, and online laboratories for science and engineering education.

Prof. del Alamo is a member of the Royal Spanish Academy of Engineering. He currently serves as Editor for the IEEE ELECTRON DEVICE LETTERS. He was a National Science Foundation Presidential Young Investigator.